Ensemble Brightening and Enhanced Quantum Yield in Size-Purified Silicon Nanocrystals

Joseph B. Miller,[†] Austin R. Van Sickle,[†] Rebecca J. Anthony,[‡] Daniel M. Kroll,[†] Uwe R. Kortshagen,[‡] and Erik K. Hobbie[†,*]

[†]Department of Physics and Department of Coatings and Polymeric Materials, North Dakota State University, Fargo, North Dakota 58108, United States and [‡]Department of Mechanical Engineering, University of Minnesota, Minneapolis, Minnesota 55455, United States

ABSTRACT

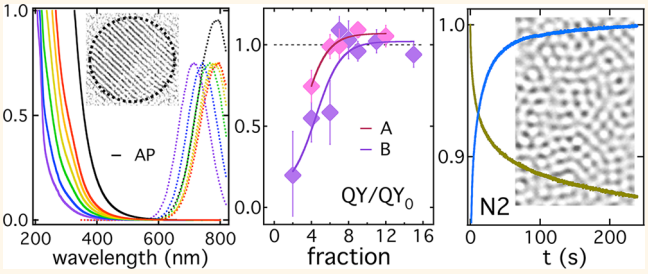

We report on the quantum yield, photoluminescence (PL) lifetime, and ensemble photoluminescent stability of highly monodisperse plasma-synthesized silicon nanocrystals (SiNCs) prepared though density-gradient ultracentrifugation in mixed organic solvents. Improved size uniformity leads to a reduction in PL line width and the emergence of entropic order in dry nanocrystal films. We find excellent agreement with the anticipated trends of quantum confinement in nanocrystalline silicon, with a solution quantum yield that is independent of nanocrystal size for the larger fractions but decreases dramatically with size for the smaller fractions. We also find a significant PL enhancement in films assembled from the fractions, and we use a combination of measurement, simulation, and modeling to link this "brightening" to a temporally enhanced quantum yield arising from SiNC interactions in ordered ensembles of monodisperse nanocrystals. Using an appropriate excitation scheme, we exploit this enhancement to achieve photostable emission.

KEYWORDS: nanocrystalline silicon · polydispersity · photoluminescent stability · quantum yield

The unique optical and electronic properties of semiconductor nanocrystals have generated a tremendous amount of research directed at a broad range of potential optoelectronic[1] and biomedical[2,3] applications. By far, the majority of the emphasis has been on nanocrystals synthesized in solution from precursors of binary alloys such as cadmium selenide (CdSe). Growing concern about the potential environmental impact of the heavy metal chalcogenides,[4,5] however, has generated considerable recent interest in alternatives. One material with exceptional promise in this regard is silicon, an abundant material that can be readily synthesized into nanocrystalline form through a number of different approaches.[6−12] Although photoluminescence (PL) due to quantum confinement in silicon was first reported over twenty years ago,[13,14] the significant technological potential of nanocrystalline silicon has only just started to emerge.[15−20] In particular, absolute PL quantum yields (QYs) as high as 60% have been reported for colloidal silicon nanocrystals (SiNCs) synthesized through a nonthermal low-pressure plasma reaction,[6,21−24] which represents the highest ensemble QY measured for SiNCs.

Despite this potential, there are significant issues that can render SiNCs less attractive than their metal−chalcogenide counterparts. Size polydispersity can result from some synthetic schemes, and several relevant methods of size purification have recently been explored.[10,11,25,26] A deeper issue, however, is the indirect band gap of silicon, which gives rise to a relatively strong thermal broadening of the PL. Because size polydispersity leads to the same type of spectral broadening, the two effects are often difficult to fully discriminate. This is particularly relevant to biomedical tagging applications, where emission spectra must be sufficiently isolated to permit color discrimination across multiple distinct channels. Like all quantum dots, SiNCs also exhibit fluorescence intermittency, or "blinking", whereby an individual nanocrystal randomly goes "dark" for time intervals varying from microseconds to minutes.[27] The generally accepted scenario implicates fluctuating surface charge states that inhibit radiative recombination.[28] For applications that seek to exploit the PL from nanocrystal

* Address correspondence to erik.hobbie@ndsu.edu.

Received for review June 7, 2012 and accepted July 18, 2012.

Published online July 18, 2012
10.1021/nn302524k

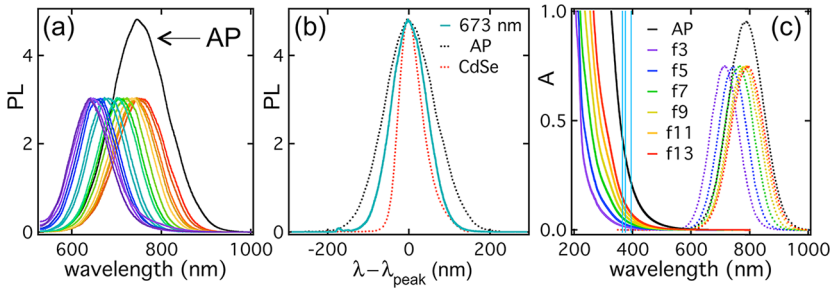

Figure 1. (a) PL spectra from solid films of the fractions and starting material (AP) for sample C. (b) Typical fraction line shape (solid blue) compared with the parent population (dashed black) and a commercially available red-NIR-emitting metal chalcogenide (dashed red). (c) Extinction spectra of typical fractions and the parent material (AP) with the corresponding emission spectra for solutions of sample B. The excitation lines used in the study are indicated in blue.

ensembles, an undesirable consequence of this emission bistability is reversible photobleaching due to the accumulation of long-lived dark states under continuous illumination.[27,28]

For SiNCs to become a competitive alternative, they will thus need to achieve levels of size uniformity, PL efficiency, and PL stability that are at least comparable to the metal chalcogenides. Motivated by this, we report on the QY and photoluminescent stability of size-purified plasma-synthesized SiNCs. We find excellent agreement with the anticipated trends of quantum confinement in silicon, with a solution QY that is relatively independent of nanocrystal size for the larger fractions but decreases rapidly with size for the smaller fractions. Spectral line widths in the best fractions are reduced by more than 30% with respect to the parent, while dried films exhibit packing order characteristic of entropic crystallization in monodisperse colloidal suspensions. Most strikingly, we find a significant PL enhancement in films assembled from the fractions, and we exploit this effect to achieve photostable emission. We use a combination of measurement, simulation, and modeling to link this "brightening" to a temporally enhanced quantum yield arising from SiNC interactions in ordered ensembles of monodisperse nanocrystals. Our results suggest that size purification applied to high-quality SiNCs is capable of producing environmentally benign semiconductor nanocrystals that can begin to match the performance of the metal chalcogenides.

RESULTS AND DISCUSSION

Although some questions remain about the exact role of surface states,[29,30] the most basic manifestations of quantum confinement in silicon are well established.[31−33] In addition to a strong dependence of the emission energy on particle size, the indirect nature of the band gap becomes somewhat tempered by electron−hole overlap, which leads to a faster recombination rate and a reduction in the number of nonradiative events with respect to the bulk material.[34] However, virtually all SiNCs studied to date have had relatively broad size distributions, and these trends are only now being tested in monodisperse materials.[11,12] For a given synthesis scheme, a rigorous metric of SiNC quality is thus how well size-purified fractions follow the anticipated trends of quantum confinement. One recent study of size-purified solution-synthesized SiNCs reported a decrease in QY with decreasing diameter,[11] suggesting that nonradiative effects can dominate quantum confinement in the limit of small nanocrystal size. Another recent study that used similar chemistry to produce larger nanocrystals reported the opposite trend,[12] however, suggesting that there is an optimum window of size for any specific synthesis scheme. The materials we use here are plasma-synthesized SiNCs capped with 1-dodecene. The mean nanocrystal size is 3−4 nm with a standard deviation of around 0.7 nm (polydispersity index of 1.05), which is exemplary for as-produced (AP) SiNCs. The crystallinity of the nanoparticles is in excellent accord with the crystalline structure of silicon (Supporting Information).[35]

Size purification was achieved through density-gradient ultracentrifugation (DGU) in mixed organic solvents using polyvinylidene fluoride ultracentrifuge tubes (Supporting Information). Increasing fraction number corresponds to greater depth in the gradient and hence larger SiNC size. Results of a typical separation are shown in Figure 1. The exact evolution of nanocrystal characteristics with fraction number varies—depending on details of the separation, the initial size distribution, and the age of the parent suspension—but the overall trends are the same. For the separation in Figure 1, the uppermost fractions (1−8) contain smaller SiNCs and impurities, while the middle fractions (9−22) contain monodisperse SiNCs of varied size. The lower fractions (>23) are populated by aggregates and larger particles and are spectrally similar to the parent. As determined by transmission electron microscopy (TEM), typical size polydispersity in the middle fractions is 1.01 (Supporting Information), corresponding to a standard deviation of 0.35 nm. High contrast in conventional TEM was achieved by draping SiNC monolayers over microscopic holes in TEM grids, as described in the Supporting Information. Figure 1b demonstrates the degree of line narrowing that can be

achieved through DGU, as referenced to both the AP material and a commercially available red/NIR-emitting metal chalcogenide.[36]

Figure 2 shows TEM images and a plot of nanocrystal diameter *versus* the energy of peak emission (365 nm excitation) for a typical separation. The solid blue curve is a fit to[31] $E = E_0 + 3.73/(2R)^{1.39}$ with the fitting parameter E_0 = 1.17 eV. The dashed curve is the analogous expression based on the band gap of bulk silicon (E_0 = 1.12 eV). Using lower energy excitation (395−473 nm) shifts the curve toward the anticipated result (solid red, Figure 2b). Figure 3a shows the PL decay in response to a 30 ps pulse (375 nm), where the time axis has been scaled to reveal the exponential relaxation. The decay is a stretched exponential, $I(t) = I_0 \exp[-(t/\tau)^{\alpha}]$ with $\alpha \approx 0.65$, reflecting a broad distribution of relaxation pathways. The lifetime is proportional to $\exp(-E/E^*)$ with $E^* \approx 0.2$ eV (Figure 3b).[37,38] Figure 3c shows the QY as a function of nanocrystal size for two different SiNC solutions in hexane, each referenced to the absolute QY of the parent (QY_0). Solutions of the parent in 1-dodecene/mesitylene had QY_0 values of 25−30% (sample A, 3.5 nm mean size) and 45−50% (sample B, 4 nm mean size) immediately after synthesis. The QY is independent of nanocrystal size for the larger fractions but decreases dramatically with size for the smaller fractions, reminiscent of the behavior reported by Mastronardi *et al.*[11] These observations are consistent with a parent size distribution that lies on a branch near and just below the nanocrystal size corresponding to the optimum QY for Si, which also happens to be roughly equivalent to the exciton Bohr radius of Si.[32] The lifetime (inset, Figure 3b) increases monotonically with increasing size.

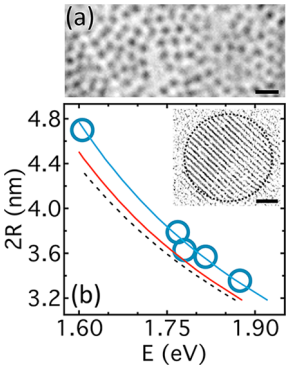

Figure 2. (a) TEM image of a typical fraction (10 nm scale). (b) Mean fraction size from TEM as a function of peak emission energy, where the blue (solid) curve is the fit described in the text (365 nm excitation), the red (solid) curve is a correction based on the measured red-shift at lower energy excitation (395−473 nm), and the dashed curve is the anticipated result based on the known band gap of bulk silicon. The inset is a TEM image of a single nanocrystal (1 nm scale). All data are from sample C.

A critical issue for many applications is the PL stability of films, which is influenced by both environment and film morphology. Reversible photobleaching arises from PL intermittency ("blinking") and the statistical buildup of long-lived "dark'" states under continuous illumination (Figure 4a−c).[27] For SiNCs, the excited singlet states of molecular oxygen efficiently quench the PL, and there is thus significant "bleaching" in air.[39] In contrast, the films are considerably more stable in nitrogen (Figure 4c−e). Nanocrystals exposed to air also blueshift over time in an irreversible fashion (Figure 4e), consistent with the gradual formation of an oxide shell.[40] A meaningful evaluation of PL stability therefore requires that the materials never be exposed to oxygen, and the films were typically cast from solution and immediately characterized under an atmosphere of flowing purified nitrogen (N_2) gas.

The morphology of the films, on the other hand, is strongly influenced by the size distribution. Previous studies of entropic self-assembly in CdSe nanocrystal suspensions highlight the importance of size uniformity for the growth of ordered superstructures,[41] while kinetic Monte Carlo simulations of colloidal crystallization suggest that the free energy of the solid−liquid interface increases strongly with supersaturation in polydisperse suspensions.[42] The standard deviation in particle size must be less than 12% of the mean for entropic crystallization to occur (corresponding to a critical polydispersity index of 1.02),[42] and size distributions comparable to those attained here will thus be

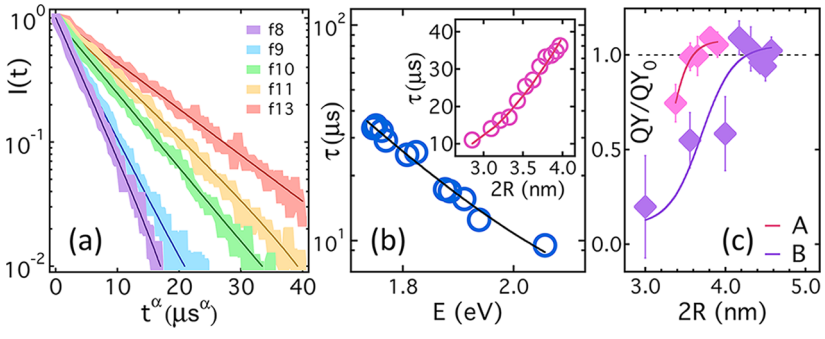

Figure 3. (a) Typical fits used to extract PL lifetime for sample C, where the stretching exponent $\alpha \approx 0.65$. (b) PL lifetime as a function of peak emission and nanocrystal size (inset) for sample C. (c) Solution quantum yield (395 nm excitation) of samples A and B referenced to the parent suspension, where the sigmoidal fits are based on a simple logistic equation.

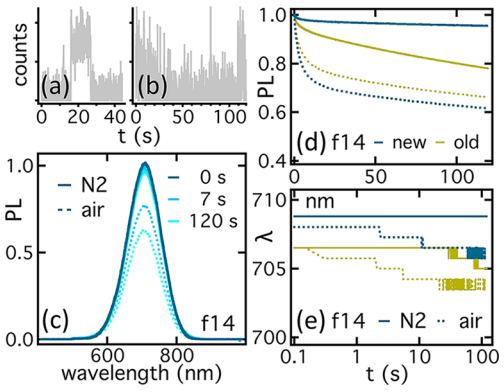

Figure 4. (a) 10 s "on" interval for a single SiNC in air. (b) 120 s trace of PL intermittency from a small (3−5 dot) assembly in air. (c) Reversible spectral "bleaching" in air (dashed) and N_2 (solid) for f14. (d) Decay of normalized PL (f14) in air (dashed) and N_2 (solid) for SiNCs never exposed directly to air ("new", blue) and the same film after 2 weeks in air ("old", green). (e) Evolution of peak PL wavelength (f14) in air (dashed) and N_2 (solid) for SiNCs never exposed directly to air ("new", blue) and the same film after 2 weeks in air ("old", green). Excitation power in (c), (d), and (e) is 0.28 W/cm^2, and all data correspond to sample C. The horizontal time label in (e) also applies to (d).

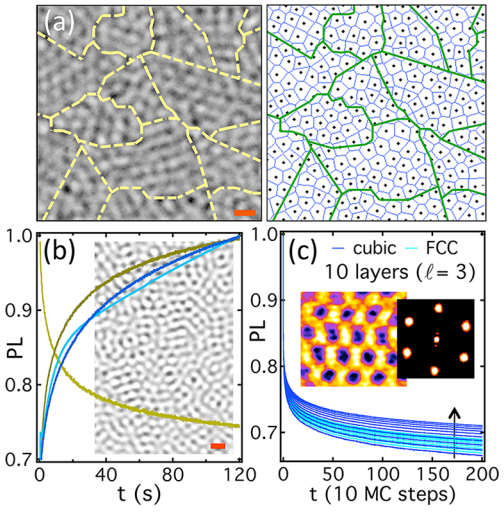

Figure 5. (a) Raw TEM image of a fraction (left) with grain boundaries and the corresponding Voronoi pattern (right). (b) PLE (f5, sample B) at low (dark blue, 0.12 W/cm^2) and moderate (light blue, 0.70 W/cm^2) power, with brightening and bleaching for the parent in compact (dark green) and sparse (light green) morphologies, respectively. Data were taken under N_2 (365 nm excitation), and the inset is a typical TEM image of a fraction. (c) MC simulation of photobleaching for 1−10 layers in simple cubic and fcc pyramidal packing with an extinction length of 3 layers. Each trace corresponds to an additional layer, and the arrow indicates increasing thickness. The inset shows a filtered TEM image of locally ordered close packing and the corresponding FFT. The scale bar in (a) and (b) is 10 nm, and the width of the real-space image in (c) is 50 nm.

essential for promoting SiNC self-assembly. The tendency for entropic crystallization in dried fractions can be seen in Figure 5a. The raw TEM image on the left shows a monolayer of size-purified SiNCs cast from toluene, and the corresponding Voronoi diagram on the right shows the packing arrangement. A pair-correlation analysis (Supporting Information) gives a nearest-neighbor spacing that is 1−1.5 nm larger than the mean nanocrystal diameter, consistent with packing stabilized by 1-dodecene. What is most striking about this image is the degree of crystallinity, even though the film was cast rapidly (50−100 s) from solvent. The equilibrium phase behaviors of the parent and fractions are detailed in the Supporting Information. To promote ordering, the films were dried at a controlled rate on a partially wetting surface.

A significant observation for such films is ensemble "brightening" under continuous illumination, reminiscent of the photobrightening that has been well documented for the metal chalcogenides.[43−55] Here, the change in PL stability correlates with a difference in film morphology; less dense regions bleach, while packed regions brighten, and the trends in Figure 5b reflect a greater tendency for the monodisperse fractions to self-assemble into 3D close-packed structures. Examples of these two distinct morphologies are given in the Supporting Information. Regions of film cast from the parent material with the same "dense" packing morphology, although uncommon, can also show brightening. We define a brightening interval as the duration over which the PL increases under continuous illumination. Figure 6a shows the measured brightening interval in the plane of excitation power and ensemble size for fraction 13 (sample B). At fixed power, the interval increases with increasing size. For fixed size, the interval decreases with increasing excitation power. For sufficiently large assemblies excited at sufficiently low power, the increase can continue on for many minutes (up to over an hour). The brightening can also persist without excitation, as previously observed for CdSe.[49]

Brightening in the metal chalcogenides has been attributed to either photoconditioning, where the photochemistry of individual nanocrystals changes under illumination,[50] or PL activation, where a "dark" fraction gradually turns "on".[56] Although we never observe brightening in sparse SiNC films or solutions, the finite optical extinction length of silicon (10 nm at 365 nm)[57]—and the subsequently delayed onset of PL in dense films—is a possible source of activation. To test this, we performed Monte Carlo simulations of PL in ordered ensembles of noninteracting SiNCs.[27] The absorption cross sections of the "dark" and "bright" states are assumed to be equivalent,[58] with a power that decays exponentially with depth and an initial PL proportional to power. The simulated ensemble PL decays as $I(t) \propto t^{-\beta}$, where the exponent β is empirically fixed from measurements of sparse films under N_2 (Supporting Information). The results for simple cubic and face-centered cubic (fcc) packing (Figure 5c) suggest enhanced PL stability with increasing film thickness, but there is no indication of brightening.

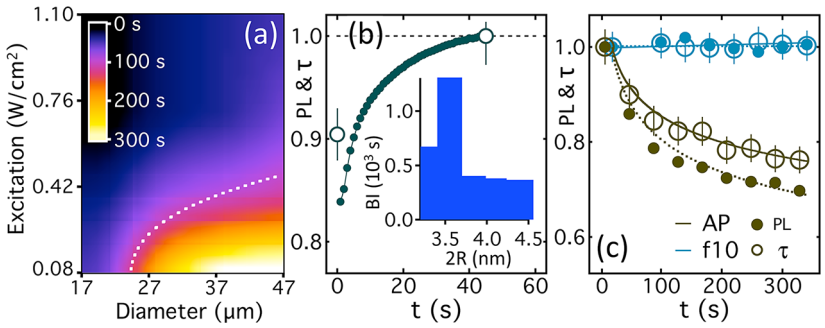

Figure 6. (a) Brightening interval (f13, sample B) in the plane of excitation power (375 nm) and ensemble size with the fit as described in the text. (b) Brightening (f10, sample B) under continuous illumination at 365 nm (115 mW/cm^2), where the open circles denote τ (normalized by final value) before and after the illumination interval. Data represent an ensemble average of multiple spots under N_2. The inset shows brightening interval (BI) in units of 10^3 s as a function of nanocrystal diameter for fractions from sample B at comparable ensemble size and excitation power (50 μm and 80 mW/cm^2). (c) PL and τ (normalized by initial values) during a bleach for the parent and for a photostable ensemble from f10 (sample B). PL and τ were measured simultaneously under N_2 with modulated pulsed excitation (375 nm, 1 kHz, 30 ps pulse width, 67 mW/cm^2 mean excitation power).

We suggest that electronic interactions between surface trap states in ordered arrays of monodisperse SiNCs increase the likelihood of radiative recombination, thereby enhancing the QY of the ensemble. A similar mechanism has been proposed for the metal chalcogenides.[46,47,49,52] In terms of kinetics, the QY is $k_r/(k_r + k_{nr})$, where k_r and k_{nr} are rate constants associated with radiative and nonradiative relaxation, respectively. These equilibrium constants define both the lifetime, $\tau = (k_r + k_{nr})^{-1}$, and the radiative lifetime, $\tau_r = k_r^{-1}$, with QY $\propto \tau$ for a specific fraction in a given morphology. By simultaneously measuring PL and τ during brightening/bleaching (Figure 6b,c), we tested the link between brightening and QY. Figure 6b shows brightening under continuous excitation, with lifetime both before and after the interval of illumination, for a film assembled from a fraction. There is a significant increase in τ, consistent with an increase in QY. Conversely, continuous excitation with a modulated pulsed laser confirms a drop in τ during bleaching for a film assembled from the parent (Figure 6c). A significant implication of this is photostable luminescence in response to an appropriately pulsed excitation, as we demonstrate in Figure 6c for a film from f10, sample B.

How reduced polydispersity promotes brightening is an intriguing question. Previous studies of CdSe films suggest that "dark" surface trap states can be passivated by slowly diffusing photoelectrons, thereby increasing the QY of the ensemble.[49] We propose a similar mechanism. The quasi-static rate of change of the QY is $-\tau^2(dk_{nr}/dt)/\tau_r$, with bleaching for $dk_{nr}/dt > 0$ and brightening for $dk_{nr}/dt < 0$. For a cubic ensemble of size L, the power density is $pL^2/L^3 = p/L$, where p is the excitation power per unit area. We assume there are two competing terms in dk_{nr}/dt, with

$$\frac{dk_{nr}}{dt} = \frac{ap}{L} - \frac{bp}{L}L^{\delta} \qquad (1)$$

where the first term models the rate of trap (dark state) production and the second, also proportional to power density, models the rate of trap annihilation. The factor of L^{δ} ($\delta > 0$) models the measured positive correlation between ensemble size and brightening interval. At large power and small size, eq 1 is dominated by the positive (bleaching) term, while the negative (brightening) term dominates for small power and large size. Setting $dk_{nr}/dt = 0$ gives the transition, with brightening above a critical size, $L_c = (a/b)^{1/\delta}$, independent of power. Well into the brightening regime, the brightening interval is $L^{1-\delta}(bp)^{-1}$. The data in Figure 6a are in good qualitative agreement with this simple model. The onset of brightening coincides with a critical length scale ($L_c \approx 18-25$ μm) that depends only weakly on power, the brightening interval increases as $1/p$ at large L, and the data are consistent with $\delta = 0.70$ [dashed curve, Figure 6a, with the contour of the constant brightening interval defined by $p \propto (L - L_c)^{1-\delta}$].

Interactions are paramount, being the source of the second term in eq 1. The rate at which trap states interact and annihilate depends on how fast they move through the ensemble, which the data suggest increases with increasing ensemble size. At comparable ensemble size and excitation power, the data also suggest that the brightening is more pronounced for smaller nanocrystals (inset, Figure 6b), although the trend might be limited here by the rapid drop in QY at small diameters. A significant consequence of size purification will be "band alignment", and when the energy states of individual SiNCs are well matched, there will be fewer inhomogeneities to impede the motion of electrons. The length of the ligand is also critical, as it dictates nanocrystal separation.[59] Samples prepared from the same fractions but with varied drying times (25 s up to 225 s) showed a direct correlation between longer drying time, longer brightening interval, and increased colloidal crystallization. Using polystyrene as a "depletant" to induce phase separation into disordered (amorphous) SiNC and polymer phases (Supporting Information), we were able to simultaneously suppress entropic crystallization and

brightening, suggesting that ordered nanocrystal packing might make a significant contribution to the L^{δ} term in eq 1. Although further study is warranted, it is conceivable that structural order could enhance the transport properties of the ensemble.

CONCLUSIONS

In conclusion, the quantum yield, photoluminescence lifetime, and ensemble photoluminescent stability of size-purified silicon nanocrystals have been measured as a function of nanocrystal size. Density-gradient ultracentrifugation in fluoropolymer centrifuge tubes has been used to generate highly monodisperse fractions of ligand-capped plasma-synthesized SiNCs, which we have optically characterized in solutions and self-assembled films. Improved size uniformity results in both reduced emission line width and an increased tendency for ordered close packing in dried nanocrystal films. We find excellent agreement with the anticipated trends of quantum confinement in nanocrystalline silicon, and the dependence of quantum yield on fraction number is consistent with an optimum nanocrystal size.

A significant PL enhancement is observed in films assembled from the fractions, which we attribute to an increase in quantum yield mediated by particle interactions in ordered ensembles of monodisperse SiNCs. Brightening was observed independent of nanocrystal size, being most dramatic for smaller fractions that still exhibited high QY. Size uniformity ensures that the individual energy bands are well aligned, which will optimize electronic overlap in the wave function of neighboring nanocrystals. Our measurements further suggest that entropic order may play a significant role in this enhancement. Motivated to a significant extent by the environmentally benign nature of silicon, many-particle photo-optical effects in silicon nanocrystals are receiving significant computational and theoretical attention.[60,61] One recent study suggested that interassembly exciton transport can be strongly influenced by nanocrystal size, suggesting the possibility of designing nanocrystal ensembles through which excitons can travel efficiently for long distances.[60] Our data also appear to suggest that nanocrystal diameter influences the response of the ensemble, and we hope that the results we present here will help stimulate further study.

The measurements we present here suggest that brightening and bleaching in SiNC ensembles are directly linked to a dynamic increase and decrease, respectively, in the quantum yield of the ensemble. The latter effect is obvious, since the accumulation of long-lived dark states under continuous illumination will by definition lead to a reduced QY, particularly if the absorption cross section changes little between the "on" and "off" states (which would presumably be the case for Auger-like quenching and transport of any subsequently generated excitons). The time dependence of brightening, in contrast, is more complex. Almost immediately after the excitation is introduced, the rate constant k_{nr} must start to decrease. A "fresh" ensemble must therefore respond instantaneously as a superposition of independent nanocrystals, but very shortly thereafter the influence of interactions emerges and the density of extended "on" states increases accordingly. Evidence for this simple picture can be found in the photoresponse of ensembles that have been briefly exposed to air, which show a short (1−10 s) interval of bleaching before the onset of brightening. A detailed study of how the enhanced PL evolves with cluster size and symmetry—from individual intermittent nanocrystals to small dense clusters of varied shape—will be reported elsewhere. The implications are potentially significant, however, since we demonstrate that the photostability and quantum yield of SiNC clusters can be controlled through self-assembly in monodisperse SiNC suspensions.

MATERIALS AND METHODS

Materials. Single-crystal silicon nanoparticles of controlled size were synthesized through a nonthermal low-pressure plasma reaction as described in detail elsewhere.[21] Three different batches were studied (denoted A, B, and C) in the size range 3−4 nm. The nanoparticles were surface processed with a 5:1 mixture of mesitylene and a ligand (1-dodecene) through a liquid-phase thermal hydrosilylation reaction that imparts colloidal stability in common organic solvents. The SiNCs were further purified by size using DGU as detailed in the Supporting Information. Density gradients of mixed chloroform and *m*-xylene were prepared in polyvinylidene fluoride ultracentrifuge tubes, with a top layer of as-produced SiNCs in *m*-xylene. Polystyrene of molecular weight 18 000 (R_g of 3.5 nm and an overlap concentration of 13%) was used as entropic depletant in SiNC−toluene solutions to induce the formation of disordered nanocrystal solids. Optical measurements of SiNC−hexane solutions were performed using quartz or glass cuvettes, and thin solid films were prepared on quartz or glass coverslips. The coverslips were UVO plasma cleaned and then annealed in perfluorodecyltriethoxysilane vapor to generate a fluorinated self-assembled monolayer, which enables control of SiNC self-assembly and packing morphology through the rate of solvent evaporation on a partially wetting surface. Additional details are given in the Supporting Information.

Methods. Transmission electron microscopy images were taken with a JEOL JEM-2100 analytical TEM operated at 200 kV and collected using a GATAN Orius SC1000 bottom-mount CCD. Quantifoil grids with an orthogonal array of microscale holes on 200 mesh copper were cleaned with chloroform and toluene, dried under vacuum, and placed on a UVO plasma-cleaned glass coverslip. A small volume (10 μL) of water was dropped onto the grid, followed by 20 μL of SiNC−toluene solution. The toluene quickly evaporates, followed by the water, leaving a monolayer of SiNCs draped over the holes in the grid. Optical measurements were generated using nearly simultaneous visible/NIR fluorescent imaging and NIR fluorescence and lifetime spectroscopy on customized inverted and upright microscopes.

Collimated variable-power fiber-coupled LEDs (365 and 395 nm) and a fiber-coupled 20 mW Omicron PhoxX 375 nm laser were used for CW excitation. Modulated pulsed excitation was delivered with a fiber-coupled pulsed UV laser (Advanced Laser Diode Systems, PiL037, 375 nm, 30 ps pulse width, 140 mW peak power, 1 kHz modulation) fiber coupled to a photomultiplier tube (Hamamatsu H10721-20) and read with a digital oscilloscope using Labview. UV–vis–NIR absorption/extinction was measured with a commercial spectrometer for both solutions and thin films. For the solutions, absolute QY was measured using a fiber-coupled 395 nm LED and an integrating sphere. Where indicated, measurements were taken using an optical cell with an exhaust valve and an intake port connected through a pressure valve to a tank of purified nitrogen (N_2). Monte Carlo (MC) simulations were performed with a discrete-time MC procedure. More details of the methods and procedures are given in the Supporting Information.

Conflict of Interest: The authors declare no competing financial interest.

Acknowledgment. E.K.H. acknowledges the support of the NSF through CBET-1133135 and the DOE through DE-FG36-08GO88160. R.J.A. and U.R.K. acknowledge primary support through the NSF under MRSEC grant DMR-0819885. We thank Christopher Moore for assistance with the measurements.

Supporting Information Available: Details of XRD characterization, DGU separation, sample preparation/morphology, TEM, absolute QY measurement, MC simulations, equilibrium phase behavior, and polymer-SiNC phase behavior are provided. This material is available free of charge *via* the Internet at http://pubs.acs.org.

REFERENCES AND NOTES

1. Ledentsov, N. N.; Ustinov, V. M.; Shchukin, V. A.; Kop'ev, P. S.; Alferov, Zh. I.; Bimbe, D. Quantum Dot Heterostructures: Fabrication, Properties, Lasers. *Semiconductors* **1998**, *32*, 343–365.
2. Medintz, I. L.; Uyeda, H. T.; Goldman, E. R.; Mattoussi, H. Quantum Dot Bioconjugates for Imaging, Labelling and Sensing. *Nat. Mater.* **2005**, *4*, 435–446.
3. Chan, W. C. W.; Nie, S. Quantum Dot Bioconjugates for Ultrasensitive Nonisotopic Detection. *Science* **1998**, *281*, 2016–2018.
4. Kirchner, C.; Liedl, T.; Kudera, S.; Pellegrino, T.; Javier, A. M.; Gaub, H. E.; Stölzle, S.; Fertig, N.; Parak, W. J. Cytotoxicity of Colloidal CdSe and CdSe/ZnS Nanoparticles. *Nano Lett.* **2005**, *5*, 331–338.
5. Derfus, A. M.; Chan, W. C. W.; Bhatia, S. N. Probing the Cytotoxicity of Semiconductor Quantum Dots. *Nano Lett.* **2004**, *4*, 11–18.
6. Jurbergs, D.; Rogojina, E.; Mangolini, L.; Kortshagen, U. Silicon Nanocrystals with Ensemble Quantum Yields Exceeding 60%. *Appl. Phys. Lett.* **2006**, *88*, 233116.
7. Liu, S. M.; Yang, Y.; Sato, S.; Kimura, K. Enhanced Photoluminescence from Si Nano-organosols by Functionalization with Alkenes and Their Size Evolution. *Chem. Mater.* **2006**, *18*, 637–642.
8. Zou, J.; Sanelle, P.; Pettigrew, K. A.; Kauzlarich, S. M. Size and Spectroscopy of Silicon Nanoparticles Prepared *via* Reduction of $SiCl_4$. *J. Cluster Sci.* **2006**, *17*, 565–578.
9. Belomoin, G.; Therrien, J.; Nayfeh, M. Oxide and Hydrogen Capped Ultrasmall Blue Luminescent Si Nanoparticles. *Appl. Phys. Lett.* **2000**, *77*, 779–782.
10. Mastronardi, M. L.; Hennrich, F.; Henderson, E. J.; Maier-Flaig, F.; Blum, C.; Reichenbach, J.; Lemmer, U.; Kübel, C.; Wang, D.; Kappes, M. M.; *et al*. Preparation of Monodisperse Silicon Nanocrystals Using Density Gradient Ultracentrifugation. *J. Am. Chem. Soc.* **2011**, *133*, 11928–11931.
11. Mastronardi, M. L.; Maier-Flaig, F.; Faulkner, D.; Henderson, E. J.; Kübel, C.; Lemmer, U.; Ozin, G. A. Size-Dependent Absolute Quantum Yields for Size-Separated Colloidally-Stable Silicon Nanocrystals. *Nano Lett.* **2012**, *12*, 337–342.
12. Hessel, C. M.; Reid, D.; Panthani, M. G.; Rasch, M. R.; Goodfellow, B. W.; Wei, J.; Fujii, H.; Akhavan, V.; Korgel, B. A. Synthesis of Ligand-Stabilized Silicon Nanocrystals with Size-Dependent Photoluminescence Spanning Visible to Near-Infrared Wavelengths. *Chem. Mater.* **2012**, *23*, 393–401.
13. Canham, L. T. Silicon Quantum Wire Array Fabrication by Electrochemical and Chemical Dissolution of Wafers. *Appl. Phys. Lett.* **1990**, *57*, 1046–1049.
14. Lehmann, V.; Gösele, U. Porous Silicon Formation: A Quantum Wire Effect. *Appl. Phys. Lett.* **1991**, *58*, 856–859.
15. Erogbogbo, F.; Yong, K.-T.; Roy, I.; Xu, G.; Prasad, P. N.; Swihart, M. T. Biocompatible Luminescent Silicon Quantum Dots for Imaging of Cancer Cells. *ACS Nano* **2008**, *2*, 873–878.
16. Fujioka, K.; Hiruoka, M.; Sato, K.; Manabe, N.; Miyasaka, R.; Hanada, S.; Hoshino, A.; Tilley, R. D.; Manome, Y.; Hirakuri, K.; *et al*. Luminescent Passive-Oxidized Silicon Quantum Dots as Biological Staining Labels and Their Cytotoxicity Effects at High Concentration. *Nanotechnology* **2008**, *19*, 415102.
17. Ding, Z.; Quinn, B. M.; Haram, S. K.; Pell, L. E.; Korgel, B. A.; Bard, A. J. Electrochemistry and Electrogenerated Chemiluminescence from Silicon Nanocrystal Quantum Dots. *Science* **2002**, *296*, 1293–1297.
18. Warner, J. H.; Hoshino, A.; Yamamoto, K.; Tilley, R. D. Water-Soluble Photoluminescent Silicon Quantum Dots. *Angew. Chem., Int. Ed.* **2005**, *117*, 4626–4630.
19. Park, J.-H.; Gu, L.; Maltzahn, G.; Ruoslahti, E.; Bhatia, S. N.; Sailor, M. J. Biodegradable Luminescent Porous Silicon Nanoparticles for *in Vivo* Applications. *Nat. Mater.* **2009**, *8*, 331–336.
20. Liu, C.-Y.; Holman, Z. C.; Kortshagen, U. R. Hybrid Solar Cells from P3HT and Silicon Nanocrystals. *Nano Lett.* **2009**, *9*, 449–452.
21. Mangolini, L.; Kortshagen, U. Plasma-Assisted Synthesis of Silicon Nanocrystal Inks. *Adv. Mater.* **2007**, *19*, 2513–2519.
22. Mangolini, L.; Jurbergs, D.; Rogojina, E.; Kortshagen, U. High Efficiency Photoluminescence from Silicon Nanocrystals Prepared by Plasma Synthesis and Organic Surface Passivation. *Phys. Status Solidi C* **2006**, *3*, 3975–3978.
23. Pi, X. D.; Liptak, R. W.; Nowak, J. D.; Wells, N.; Carter, C. B.; Campbell, S.; Kortshagen, U. Air-Stable Full-Visible-Spectrum Emission from Silicon Nanocrystal Ensembles Synthesized by an All-Gas-Phase Plasma Approach. *Nanotechnology* **2008**, *19*, 245603.
24. Anthony, R. J.; Rowe, D. J.; Stein, M.; Yang, J.; Kortshagen, U. Routes to Achieving High Quantum Yield Luminescence from Gas-Phase-Produced Silicon Nanocrystals. *Adv. Funct. Mater.* **2011**, *21*, 4042–4046.
25. Li, X.; He, Y.; Swihart, M. T. Surface Functionalization of Silicon Nanoparticles Produced by Laser-Driven Pyrolysis of Silane followed by $HF-HNO_3$ Etching. *Langmuir* **2004**, *20*, 4720–4727.
26. Bai, L.; Ma, X.; Liu, J.; Sun, X.; Zhao, D.; Evans, D. G. Rapid Separation and Purification of Nanoparticles in Organic Density Gradients. *J. Am. Chem. Soc.* **2010**, *132*, 2333–2337.
27. Cichos, F.; Martin, J.; von Borczyskowski, C. Emission Intermittency in Silicon Nanocrystals. *Phys. Rev. B* **2004**, *70*, 115314.
28. Lee, S. F.; Osborne, M. A. Brightening, Blinking, Bluing and Bleaching in the Life of a Quantum Dot: Friend or Foe? *Chem. Phys. Chem.* **2010**, *10*, 2174–2191.
29. Martin, J.; Cichos, F.; Huisken, F.; von Borczyskowski, C. Electron-Phonon Coupling and Localization of Excitons in Single Silicon Nanocrystals. *Nano Lett.* **2008**, *8*, 656–660.
30. Sa'ar, A.; Reichman, Y.; Dovrat, M.; Krapf, D.; Jedrzejewski, J.; Balberg, I. Resonant Coupling between Surface Vibrations and Electronic States in Silicon Nanocrystals at the Strong Confinement Regime. *Nano Lett.* **2005**, *5*, 2443–2447.
31. Ledoux, G.; Guillois, O.; Porterat, D.; Reynaud, C.; Huisken, F.; Kohn, B. Photoluminescence Properties of Silicon Nanocrystals as a Function of Their Size. *Phys. Rev. B* **2000**, *62*, 15942–15951.

32. Ledoux, G.; Gong, J.; Huisken, F.; Guillois, O.; Reynaud, C. Photoluminescence of Size-Separated Silicon Nanocrystals: Confirmation of Quantum Confinement. *Appl. Phys. Lett.* **2002**, *80*, 4834–4837.
33. Ledoux, G.; Gong, J.; Huisken, F. Effect of Passivation and Aging on the Photoluminescence of Silicon Nanocrystals. *Appl. Phys. Lett.* **2001**, *79*, 4028–4030.
34. Sykora, M.; Mangolini, L.; Schaller, R. D.; Kortshagen, U.; Jurbergs, D.; Klimov, V. I. Size-Dependent Intrinsic Radiative Decay Rates of Silicon Nanocrystals at Large Confinement Energies. *Phys. Rev. Lett.* **2008**, *100*, 067401.
35. Anthony, R.; Kortshagen, U. Photoluminescence Quantum Yields of Amorphous and Crystalline Silicon Nanoparticles. *Phys. Rev. B* **2009**, *80*, 115407.
36. The CdSe spectrum is from Qdot 705 (peak emission at 705 nm) coated with streptavidin in water at pH 7.2 (www.invitrogen.com).
37. Delerue, C.; Allan, G.; Lannoo, M. Theoretical Aspects of the Luminescence of Porous Silicon. *Phys. Rev. B* **1993**, *48*, 11024–11036.
38. Huisken, F.; Ledoux, G.; Guillois, O.; Reynaud, C. Light-Emitting Silicon Nanocrystals from Laser Pyrolysis. *Adv. Mater.* **2002**, *14*, 1861–1865.
39. Goller, B.; Polisski, S.; Wiggers, H.; Kovalev, D. Silicon Nanocrystals Dispersed in Water: Photosensitizers for Molecular Oxygen. *Appl. Phys. Lett.* **2010**, *96*, 211901.
40. English, D. S.; Pell, L. E.; Yu, Z.; Barbara, P. F.; Korgel, B. A. Size Tunable Visible Luminescence from Individual Organic Monolayer Stabilized Silicon Nanocrystal Quantum Dots. *Nano Lett.* **2002**, *2*, 681–685.
41. Murray, C. B.; Kagan, C. R.; Bawendi, M. G. Self-organization of CdSe Nanocrystallites into Three-Dimensional Quantum Dot Superlattices. *Science* **1995**, *270*, 1335–1338.
42. Auer, S.; Frenkel, D. Suppression of Crystal Nucleation in Polydisperse Colloids due to Increase of the Surface Free Energy. *Nature* **2001**, *413*, 711–713.
43. Wang, S.; Querner, C.; Fischbein, M. D.; Willis, L.; Novikov, D. S.; Crouch, C. H.; Drndic, M. Blinking Statistics Correlated with Nanoparticle Number. *Nano Lett.* **2008**, *8*, 420–426.
44. Yu, M.; Van Orden, M. Enhanced Fluorescence Intermittency of CdSe-ZnS Quantum-Dot Clusters. *Phys. Rev. Lett.* **2006**, *97*, 237402.
45. Kimura, J.; Uematsu, T.; Maenosono, S.; Yamaguchi, Y. Photoinduced Fluorescence Enhancement in Mono- and Multilayer Films of CdSe/ZnS Quantum Dots: Dependence on Intensity and Wavelength of Excitation Light. *J. Phys. Chem. B* **2005**, *109*, 8613–8618.
46. Maenosono, S. Monte Carlo Simulations of Photoinduced Fluorescence Enhancement in Semiconductor Quantum Dot Arrays. *Chem. Phys. Lett.* **2005**, *405*, 182–186.
47. Lee, J. D.; Maenosono, S. Intensified Blinking, Continuous Memory Loss, and Fluorescence Enhancement of Interacting Light-Emission Quantum Dots. *Phys. Rev. B* **2009**, *80*, 205327.
48. Wang, S.; Querner, C.; Dadosh, T.; Crouch, C. H.; Novikov, D. S.; Drndic, M. Collective Fluorescence Enhancement in Nanoparticle Clusters. *Nat. Commun.* **2011**, *2*, 364.
49. Tice, D. B.; Frederick, M. T.; Chang, R. P. H.; Weiss, E. A. Electron Migration Limits the Rate of Photobrightening in Thin Films of CdSe Quantum Dots in a Dry N_2 (g) Atmosphere. *J. Phys. Chem. C* **2011**, *115*, 3654–3662.
50. Jones, M.; Nedeljkovic, J.; Ellingson, R. J.; Nozik, A. J.; Rumbles, G. Photoenhancement of Luminescence in Colloidal CdSe Quantum Dot Solutions. *J. Phys. Chem. B* **2003**, *107*, 11346–11352.
51. Peterson, J. J.; Krauss, T. D. Photobrightening and Photodarkening in PbS Quantum Dots. *Phys. Chem. Chem. Phys.* **2006**, *8*, 3851–3856.
52. Christova, C. G.; Stouwdam, J. W.; Eijkemans, T. J.; Silov, A. Y.; van der Heijden, R. W.; Kemerink, M.; Janssen, R. A. J.; Salemink, H. W. M. Photoluminescence Enhancement in Thin Films of PbSe Nanocrystals. *Appl. Phys. Lett.* **2008**, *93*, 121906.
53. Hess, B. C.; Okhrimenko, I. G.; Davis, R. C.; Stevens, B. C.; Schulzke, Q. A.; Wright, K. C.; Bass, C. D.; Evans, C. D.; Summers, S. L. Surface Transformation and Photoinduced Recovery in CdSe Nanocrystals. *Phys. Rev. Lett.* **2001**, *86*, 3132–3135.
54. Asami, H.; Abe, Y.; Ohtsu, T.; Kamiya, I.; Hara, M. Surface State Analysis of Photobrightening in CdSe Nanocrystal Thin Films. *J. Phys. Chem. B* **2003**, *107*, 12566–12568.
55. Myung, N.; Bae, Y.; Bard, A. J. Enhancement of the Photoluminescence of CdSe Nanocrystals Dispersed in $CHCl_3$ by Oxygen Passivation of Surface States. *Nano Lett.* **2003**, *3*, 747–749.
56. Osborne, M. A.; Lee, S. F. Quantum Dot Photoluminescence Activation and Decay: Dark, Bright, and Reversible Populations in ZnS-Capped CdSe Nanocrystals. *ACS Nano* **2011**, *5*, 8295–8304.
57. Herzinger, C. M.; Johs, B.; McGahan, W. A.; Woollam, J. A.; Paulson, W. Ellipsometric Determination of Optical Constants for Silicon and Thermally Grown Silicon Dioxide *via* a Multi-Sample, Multi-Wavelength, Multi-Angle Investigation. *J. Appl. Phys.* **1998**, *83*, 3323–3337.
58. Yao, J.; Larson, D. R.; Vishwasrao, H. D.; Zipfel, W. R.; Webb, W. W. Blinking and Nonradiant Dark Fraction of Water-Soluble Quantum Dots in Aqueous Solution. *Proc. Natl. Acad. Sci. U. S. A.* **2005**, *102*, 14284–14289.
59. Knowles, K. E.; Frederick, M. T.; Tice, D. B.; Morris-Cohen, A. J.; Weiss, E. A. Colloidal Quantum Dots: Think Outside the (Particle-in-a-)Box. *J. Phys. Chem. Lett.* **2012**, *3*, 18–26.
60. Lin, Z.; Li, H.; Franceschetti, A.; Lusk, M. T. Efficient Exciton Transport between Strongly Quantum-Confined Silicon Quantum Dots. *ACS Nano* **2012**, *6*, 4029–4038.
61. Allan, G.; Delerue, C. Energy Transfer between Semiconductor Nanocrystals: Validity of Forster's Theory. *Phys. Rev. B* **2007**, *75*, 195311.